Journal of Industrial and Engineering Chemistry xxx (xxxx) xxx

Contents lists available at ScienceDirect

Journal of Industrial and Engineering Chemistry

journal homepage: www.elsevier.com/locate/jiec

Interchain hydrogen-bonded conjugated polymer for enhancing the stability of organic solar cells

Nam Gyu Yang, Sung Jae Jeon, Young Hoon Kim, Hyoung Seok Lee, Dong Hyun Hong, Doo Kyung Moon *

Nano and Information Materials (NIMs) Laboratory, Department of Chemical Engineering, Konkuk University, 120 Neungdong-ro, Gwangjin-gu, Seoul 05029, Republic of Korea

ARTICLE INFO

Article history:
Received 12 March 2022
Revised 26 April 2022
Accepted 1 May 2022
Available online xxxx

Keywords:
Organic solar cells
D-A copolymer
Thermal chain cleavage
Interchain hydrogen-bonding
UV-blocking layer
Stability

ABSTRACT

Operational stability of organic solar cells (OSCs) is a key issue for the commercialization. In order to enhance the stability of OSCs, various strategies are being used. In this study, pyrroles and isoindigo monomers with *tert*-butoxycarbonyl side chains were synthesized and used to prepare a D–A-type polymer, P(TBPyTBIID), via Stille coupling. The obtained polymer dissolved readily in organic solvents, such as chloroform. However, the formation of interchain hydrogen bonds after side-chain cleavage via thermal treatment rendered the resulting polymer insoluble in organic solvents. In addition, strong π···π stacking due to face-on orientation enabled dense packing of the structure, which led to an increase in resistances to organic solvents, acid, and ultraviolet (UV) light. P(TBPyTBIID) was introduced as a UV and external protective layer, along with silver nanoparticles, at the back surface of the glass substrate. The light-soaking stability was enhanced without significantly reducing the efficiencies of the organic solar cells. This work indicates that introducing an UV blocking layer can be an effective strategy to increase the stability of organic solar cells.

Introduction

Organic electronic devices, light-emitting diodes, and solar cells (OSCs) that use organic semiconductors are attracting considerable attention due to their low costs, light weights, flexibilities, and solution processabilities. However, the active layers of such organic electronic devices are vulnerable to light, moisture (H_2O), and oxygen due to their low energy states [1,2]. These conditions that rapidly degrade organic compounds must be strictly controlled during manufacturing and within the devices. Therefore, the design and selection of materials should be considered, in addition to device engineering, processing techniques, and encapsulation [3].

(1) In terms of material design, the stability can be enhanced via structural changes in the active or charge transport materials. In their study on adjusting the spacer length of small-molecule donors with A-π-D-π-A structures, Wang et al. reported that extended conjugation length resulted in enhanced long-term device stability [4]. Doping the interfacial material is also an effective strategy to enhance the solar cell performance. Song et al. synthesized zirconium-doped ZnO nanoparticles as a cathode interfacial layer and reported the enhancement of thickness tolerance and shelf stability [5]. (2) In terms of device engineering, a third component may be introduced to form a more stable morphology. An et al. reported that the introduction of a high-molecular-weight acceptor (N2200) as a third component into the PBDB-T:ITIC system resulted in improved stability compared to that of the binary system [6]. Yin et al. reported that the efficiency and stability improved upon incorporating 1,4-butanedithiol as an additive instead of 1,8-diiodooctane (DIO), which is an unstable, widely used additive. Additionally, additives with lower boiling points promoted the thermal stability of the active layer [7]. Song et al. reported two device engineering strategies to control the aggregation state of the active materials. By introducing volatile process-aid solid (PAS) [8], and by using tunable non-halogenated solvent engineering (TSE) [9], they successfully controlled the aggregation and morphologies of the active layers to improve the performance of the devices. (3) Encapsulating the device is another promising strategy to enhance the lifetime and mechanical stability of a device by blocking external moisture and oxygen [10]. (4) Ultraviolet (UV) light can be blocked to increase the stabilities of UV-sensitive organic semiconductors [11–14]. Lukas Schmidt-Mende et al. successfully enhanced the stability by incorporating electron transport layers (TiO_2) that effectively filtered UV light via absorption [11]. Our group incorpo-

* Corresponding author.
E-mail address: dkmoon@konkuk.ac.kr (D.K. Moon).

https://doi.org/10.1016/j.jiec.2022.05.001
1226-086X/

rated hole transport layers with multifunctional double-layered structures into UV-curing during electrode (Ag) formation. Consequently, the UV protection increased the photostability of the device [15]. Moreover, studies involving altering the side chains of molecular structures to enhance stability were reported. In general, side chains affect the solubility and optical and electronic properties of the overall molecular structure [16]. In particular, sites where hydrogen bonding may occur in side-chains bearing N–H bonds, such as diketopyrrolopyrrole (DPP), isoindigo (IID), and quinacridone derivatives, are exposed following cleavage [17–19]. Thus, the rigidity of the structure increases due to the formation of intra- or intermolecular hydrogen bonds. These dyestuffs exhibit planar structures in organic electronic devices, and the resulting high hole mobility, improved morphology, and surface optimization yield significant advantages [20]. Fang et al. used quinacridone derivatives that cleaved side chains to synthesize intermolecular hydrogen-bonding ladder polymers. These polymers showed very strong mechanical properties and solvent resistances, suggesting that they could be applied in harsh environments, such as space, and as precursors to carbon materials [21]. Huang et al. used indigo derivatives that incorporated a benzodithiophene (BDT) derivative and *tert*-butoxycarbonyl (*t*-BOC) group to synthesize a D–A-type polymer. This polymer was subsequently incorporated into the active layers of organic thin film transistors (OTFTs) and OSCs via solution processes, and improved properties were reported following the removal of the bulky *t*-BOC side groups via thermal treatment [22].

In this study, we synthesized D–A type polymer with isoindigo derivative as an acceptor-unit and pyrrole derivative as a donor-unit. We then introduced *t*-BOC chains that could be thermally cleaved at the N-sites of the isoindigo and pyrrole, followed by polymerization via Stille coupling. The obtained polymer, poly (di-*tert*-butyl-(*E*)-6-(1-(*tert*-butoxycarbonyl)-1H-pyrrol-2-yl)-2,2′-dioxo-[3,3′-biindolinylidene]-1,1′-dicarboxylate) (P(TBPyTBIID), was readily soluble in organic solvents, such as chloroform (CF). The efficiency of side chain removal based on the temperature of thermal treatment was investigated, with a 100% efficient side-chain removal occurring upon heating for 30 min at 150 °C. After the removal of the side chains, P(TBPyTBIID) exhibited a crystalline structure with strong $\pi\cdots\pi$ stacking due to the face-on orientation, which considerably increased the resistances to organic solvents, acids, and UV light. P(TBPyTBIID) was introduced as a UV and external protective layer, along with silver nanoparticles (AgNPs), to the lower surface of the glass, and the photostability was enhanced without significantly reducing the efficiency of the device.

Experimental section

Materials and instruments

All reagents and chemicals were purchased from commercial sources and used without further purification unless stated otherwise (TCI chemicals, Sigma-Aldich and Acros organics). PM6 and Y6-BO-4Cl were obtained commercially form Suna Tech Inc.

Unless otherwise specified, all reactions were performed under a nitrogen atmosphere. The solvents were dried using the standard procedures. All column chromatography was performed with silica gel (230–400 mesh, Merck) as the stationary phase. ^{1}H NMR spectrum were collected by a Bruker ARX 400 spectrometer using solutions in $CDCl_3$ with chemical concentrations recorded in ppm units using TMS as the internal standard. The absorption (UV) spectra were measured in chloroform using an HP Agilent 8453 UV–Vis spectrophotometer. The cyclic voltammetry (CV) waves were obtained using a Zahner IM6eX electrochemical workstation with a 0.1 M acetonitrile (purged with nitrogen for 20 min) solution containing tetrabutyl ammonium hexafluorophosphate (Bu4NPF6) as the electrolyte at a constant scan rate of 50 mV/s. ITO, a Pt wire, and silver/silver chloride [Ag in 0.1 M KCl] were used as the working, counter, and reference electrodes, respectively. The electrochemical potential was calibrated against Fc/Fc+. The HOMO levels of the polymers were determined using the oxidation onset value. The onset potentials are the values obtained from the intersection of the two tangents drawn at the rising current and the baseline changing current of the CV curves. Thermogravimetric analysis (TGA) measurements were performed on a NETZSCH TG 209 F3 thermogravimetric analyzer. Attenuated total reflectance Fourier transform infrared spectroscopy (ATR-FTIR) measurements were performed on a FT/IR 4100, using powdered or coated sample. All gel permeation chromatography (GPC) analyses were performed using chloroform as an eluent and a polystyrene standard as a reference. XRD patterns were obtained using a Smart Lab 3 kW (40 kV 30 mA, Cu target, wavelength: 1.541871 Å) instrument of Rigaku, Japan. The optimized molecular geometries of the model molecules were obtained by minimize energy calculations with Gaussian 09. Theoretical analyses were performed using density functional theory (DFT) as approximated by the B3LYP functional and employing the 6-31G(d) basis set.

Synthetic procedures

The synthesis of monomers were carried out by referring to and changing the previous literature [23]. Synthesis of monomers and ^{1}H NMR data are specified in supporting information.

Polymerization of P(TBPyTBIID) – (6) (24.6 mg, 0.05 mmol), **(3)** (31 mg, 0.05 mmol), Tris(dibenzylideneacetone) dipalladium (0) (1 mg, 0.0011 mmol), Tris(o-tolyl)phosphine (1.2 mg, 0.0039 mmol) were dissolved in 4 mL of tetrahydrofuran. The flask was flushed with nitrogen and the temperature was raised to 66 °C. After 120 hours of reaction, the reaction mixture was cooled down to room temperature and poured into methanol. The product was Soxhlet extracted with methanol, acetone, hexanes, methylene chloride and chloroform in a sequence. Chloroform fraction was dried and precipitated in methanol to obtain navy solid. (yield = 70%) ^{1}H NMR (400 MHz, $CDCl_3$): δ 8.84(br, 2H), 8.07(br, 2H), 7.32(br, 2H), 6.49(br, 2H), 1.64–1.59(br, 27H).

Device fabrication

Binary and ternary organic solar cell device was fabricated with the structure of ITO/PEDOT:PSS/Active layer/PDINN/Ag. Patterned ITO substrates were sonicated for 15 min and rinsed with acetone, Alconox solution, isopropanol, and deionized water in a sequence. Substrates were transferred into UVO cleaner and exposed with uv-ozone for 30 min for surface treatment. PEDOT:PSS (Heraeus, AI4083) was filtered through 0.45 μm PTFE syringe filter, and spin-coated for 60 s at 5000 rpm, and annealed for 15 min at 150 °C to form 40 nm of HTLs. Substrates were then transferred into nitrogen filled glovebox with 3 ppm of moisture, and 3 ppm of oxygen. Active layers were spin-coated onto HTLs. Active blends (1:1 of P(TBPyTBIID) and Y6-BO-4Cl with the concentration of 12 mg/mL for binary structure, and 1:0.008:1 of PM6, P(TBPyTBIID), and Y6-BO-4Cl with the concentration of 12 mg/mL for ternary structure dissolved in chlorobenzene containing 0.5 v% of chloronaphthalene) were spin-coated for 30 s at 2300 rpm onto HTLs and annealed for 10 min at 150 °C to form 100 nm of active layer. PDINN (Sunatech., 1 mg/mL in methanol) was spin-coated for 30 s at 3000 rpm to form ETLs. Substrates were then transferred into high-vacuum chamber with the pressure of 5×10^{-7} torr, and 100 nm of silver was thermally evaporated to form top electrode.

Organic solar cell devices containing UV-blocking layers were fabricated with the structure of UV-blocking layer/AgNPs/ITO/PEDOT:PSS/Active layer/PDINN/Ag. Pretreatment of the substrates were conducted with the same procedure as above. Under the substrate, AgNPs (Aldrich, diluted 100, 1000, and 10,000 times by volume in IPA) were spin-coated for 60 s at 3000 rpm and annealed for 10 min at 200 °C. P(TBPyTBIID) (5, 10 mg/mL in CF) was spin-coated for 30 s at 3000 rpm and annealed for 10 min at 200 °C to form UV-blocking layer. Substrates were transferred into UVO cleaner and exposed with uv-ozone for 30 min for surface treatment. After that, all the other procedures were same as above except for the active blend condition (1:1 of PM6 and Y6-BO-4Cl with the concentration of 12 mg/mL total in chlorobenzene containing 0.5 v% of chloronaphthalene).

Results and discussion

Molecular design and synthesis

By using building blocks bearing N–H bonds, such as diketopyrrolopyrrole (DPP), isoindigo (IID), and quinacridone derivatives, side chains can easily be attached to these N–H sites. And if N–H sites are exposed after the side chain cleavage, hydrogen bonding may occur at these. If hydrogen bonds are formed after the side chain cleavage, the rigidity of the structure increases. DPP, IID, and quinacridone units also exhibit planar structures in organic electronic devices, and the resulting high hole mobility, improved morphology, and surface optimization yield significant advantages. Thus, we introduced *t*-BOC chains that could be thermally cleaved at the N-sites of the IID and pyrrole units. The synthesis of the monomers and polymers are shown in Scheme 1 and are conducted according to literature methods, with each molecular structure identified using ^{1}H-nuclear magnetic resonance spectroscopy (see ES). The polymerization is conducted via the Stille coupling of **(6)** (*tert*-butyl 2,5-bis(trimethylstannyl)-1H-pyrrole-1-carboxylate) and **(3)** (di-*tert*-butyl (E)-6,6′-dibromo-2,2′-dioxo-[3,3′-biindolinylidene]-1,1′-dicarboxylate). The obtained polymer was a navy solid that readily dissolved in organic solvents, such as CF. The structure of the polymer is confirmed as P(TBPyTBIID) (Fig. S7).

Gel permeation chromatography (GPC) of P(TBPyTBIID) reveals a Mn and Mw of 3.47 and 4.56 kDa, respectively, with a PDI of 1.32 (Table S1).

Theoretical density functional theory (DFT) calculations using the B3LYP/6-31G(d) level functionals were conducted on the ideal structure of P(TBPyTBIID), and the results are shown in Fig. 1. The dihedral angle between the pyrrole (donor unit) and isoindigo (acceptor unit) is 49.9° prior to *t*-BOC side-chain cleavage (a,c), and 18.8° following side-chain cleavage (b,d), indicating that the structure becomes more planar after side-chain cleavage. Therefore, we expected stronger π···π stacking can be formed after *t*-BOC side-chain cleavage via thermal treatment.

Thermal cleavage of P(TBPyTBIID)

The thermal properties of the synthesized polymer were determined using thermogravimetric analysis, as shown in Fig. 2a. The mass of the polymer decreases sharply between 150 and 200 °C, which indicates the cleavage of the relatively unstable *t*-BOC side chain weakly bonded to the polymer. The molecular weights per repeating unit before and after *t*-BOC removal are shown in Table S2. The mass ratio relative to the initial mass was measured after polymer stabilization at >200 °C, with a value of 62% (38% mass loss) obtained. This mass ratio is very close to the calculated value of 65%, confirming that the cleavage of the *t*-BOC side chains occurs between 150 and 200 °C [20–23]. As the product resulting from the removal of the side chains is the product to be applied, we analyzed the thermal stability of the product.

Therefore, the temperature where another 5% mass loss occurs after the first mass loss at 200 °C was set as T_d (∼461 °C), which indicates that P(TBPyTBIID) exhibits an extremely high thermal stability. This is due to the interchain hydrogen bonds that form after the removal of the *t*-BOC side chains and the strong π···π stacking resulting from the enhanced planarity.

Chain cleavage efficiency under different annealing conditions

The cleavage of the *t*-BOC side chains generally occurs via thermal treatment at 200 °C for >10 min [20–23]. Because previous studies conducted thermal treatment at <200 °C for *t*-BOC cleavage, and the TGA thermograms occasionally confirmed the cleavage of the *t*-BOC side chains in the temperature range 150 ∼ 200 °C, we studied the efficiency of side-chain cleavage at various temperatures in the range 150 ∼ 200 °C for various durations. Thermal treatment was conducted for 10, 20, and 30 min at 150 and 175 °C and 10 and 20 min at 200 °C. The changes in solubility and the UV–visible (UV–vis) spectrum of each sample are shown in Figs. S9 and S10. In conclusion, a reduction in solubility is observed in all the samples treated at ≥150 °C, but the UV–vis spectra reveal that the cleavage efficiency is identical when the polymer is thermally treated for 30 min at 150 °C or 10 min at 200 °C.

Fig. 2b shows the Fourier transform infrared spectra of P(TBPyTBIID) with various annealing time at 200 °C. The spectrum prior to thermal treatment shows signals representing the C=O of the isoindigo backbone and the C=O of *t*-BOC at 1730 and 1780 cm^{-1}, respectively. However, the signal at 1780 cm^{-1} is decreased and finally not observed in the spectrum as annealing time increases, confirming that the *t*-BOC side chains are cleaved. A weak signal corresponding to N–H is detected at approximately 3200–3470 cm^{-1}, which is likely due to hydrogen bonding between the N–H and C=O (hydrogen bonded NH stretching vibration). In addition, the signal corresponding to the C=O of isoindigo shifts from 1730 to 1690 cm^{-1} after thermal treatment (from amide I, C=O stretching) – this is due to the hydrogen bonding between C=O and N–H weakening the C=O bond, which is consistent with previous studies [18,24–26]. Also, the amide II peak at 1600 cm^{-1} was shifted higher wavenumber to 1610 cm^{-1}, indicating that N–H bending signal confirming the formation of secondary amine consequently [27]. The interchain hydrogen bonds formed by the cleavage of the *t*-BOC side chains may also be confirmed via changes in solubility before and after thermal treatment. The polymer was coated on a glass substrate, and we compared the solubility of the polymer in CF before and after thermal treatment. As shown in Fig. 2c, the coated P(TBPyTBIID) readily dissolves in CF prior to thermal treatment but does not dissolve following thermal treatment. These changes in solubility suggest that the N–H and C=O, which are exposed after thermal treatment, interact to form interchain hydrogen bonds, leading to stronger intermolecular forces.

Optical and electrochemical properties

Fig. 3a shows the UV–vis absorption spectra of P(TBPyBIID) in solution (in CF, black line) and in film (red line: before annealing, blue line: after annealing). The spectrum of P(TBPyBIID) exhibits absorption peaks at 300–400 nm and 400–800 nm due to π-π* transition and strong intramolecular charge transfer interactions, respectively, between pyrrole and isoindigo [28,29]. The absorption peak at 400–800 nm in the spectrum measured in solution is broadened when the film is formed (450–950 nm) and after thermal treatment (400–1100 nm). The maximum absorption peaks

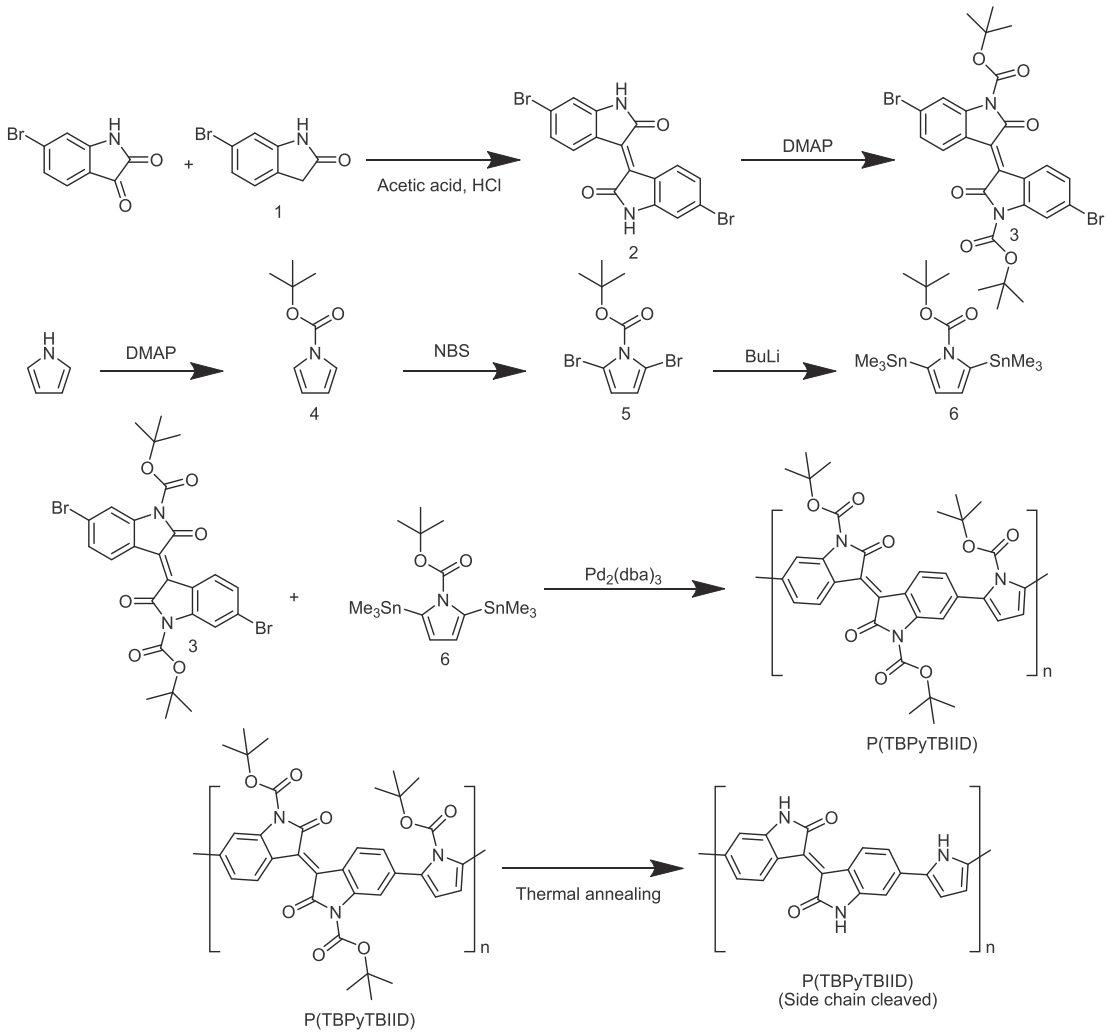

Scheme 1. Scheme for synthesis and side chain cleavage of P(TBPyTBIID).

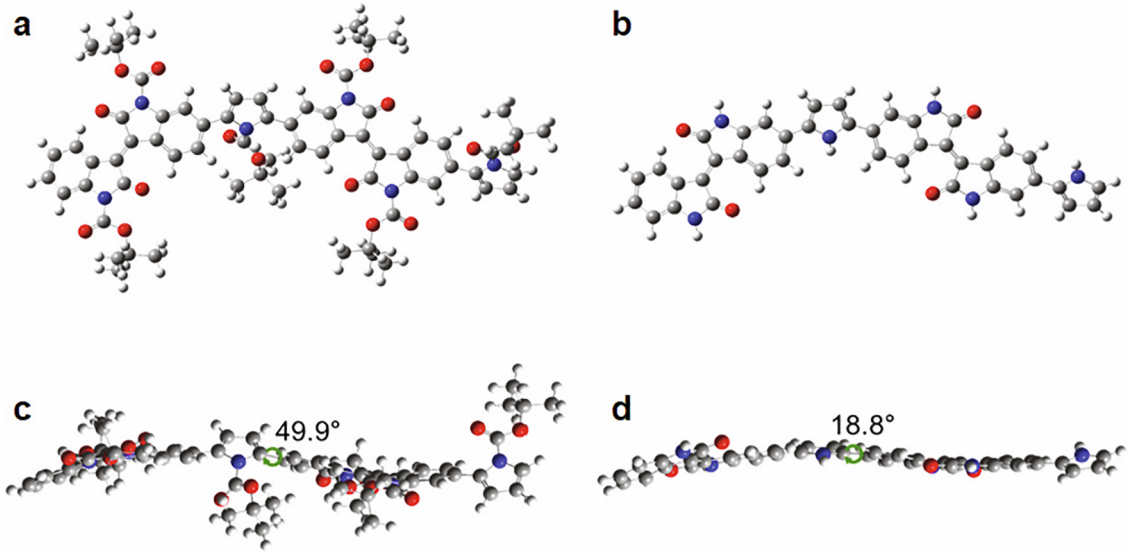

Fig. 1. Calculated molecular structure of P(TBPyTBIID); (a, b) top view, (c, d) side view.

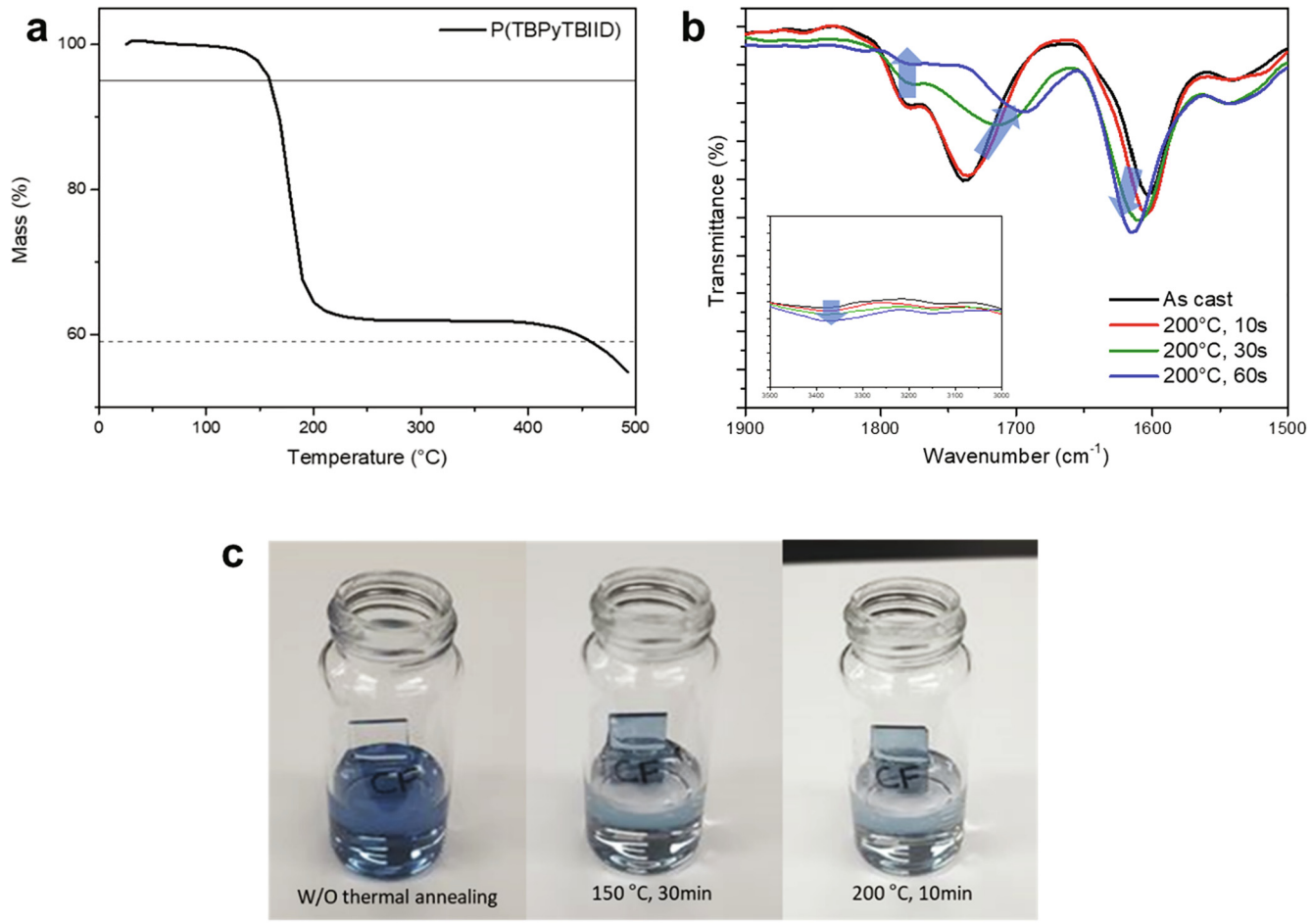

Fig. 2. (a) TGA curve of P(TBPyTBIID), (b) FT-IR spectrum of P(TBPyTBIID) with various annealing time at 200 °C, and c picture of solubility change of P(TBPyTBIID) before and after annealing.

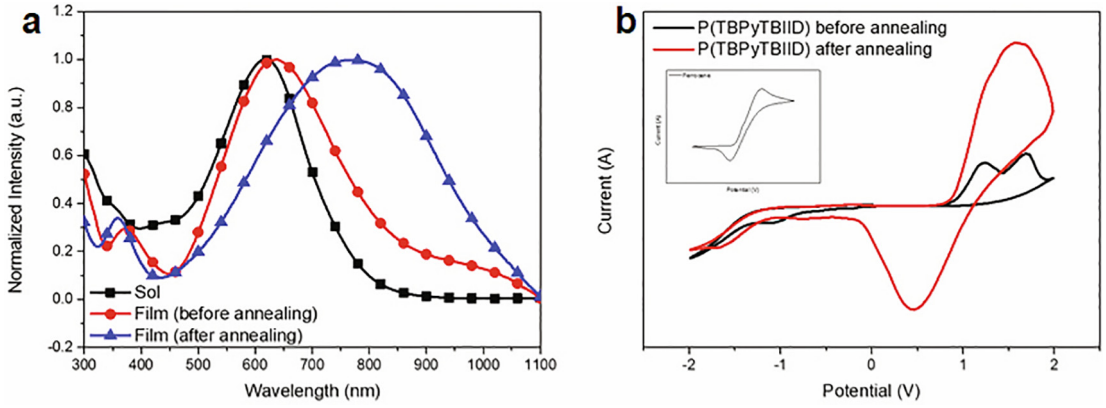

Fig. 3. (a) UV–vis spectrum of P(TBPyTBIID), (b) cyclic voltammograms of P(TBPyTBIID) before and after annealing.

(λ_{max}) are observed at 618, 637, and 765 nm, confirming that a red shift occurs.

Table 1 shows the UV–vis spectral data. The optical band gaps of P(TBPyTBIID) before and after thermal treatment are calculated using the UV–vis absorption spectrum of the film state as 1.48 and 1.22 eV, respectively. The red shifts of these absorption spectra are due to the high aggregation and packing of the molecules upon film formation. In particular, the results are consistent with the DFT results shown in Fig. 1 that reveal the more planar structure due to *t*-BOC side-chain cleavage from P(TBPyTBIID) following thermal treatment. The aggregation and π···π stacking are maximized due to the hydrogen bonds between the C = O and N–H groups, resulting in a larger red shift[30].

Fig. 3b shows the cyclic voltammogram of P(TBPyTBIID) before and after thermal treatment. The following equation is used to calculate the highest occupied molecular orbital (HOMO) level: **[HOMO(eV) = −4.8 − (E_{onset} − $E_{1/2(Ferrocene)}$)]**. The calculated HOMO values of P(TBPyTBIID) before and after thermal treatment are

Table 1
Optical and electrochemical properties of P(TBPyTBIID) before and after annealing.

Polymers	Abs. [nm]			$Eg^{Opt,a)}$ [eV]	Energy level			
	Solution	Film			CV		DFT	
	λ_{max}	λ_{max}	λ_{onset}		HOMO [eV]	LUMO [eV]	HOMO [eV]	LUMO [eV]
P(TBPyTBIID) Before annealing	618	372, 637	838	1.48	5.22	3.74	5.11	3.01
P(TBPyTBIID) After annealing	-	359, 765	1016	1.22	5.23	4.01	4.95	2.84

[a)] Calculated from the intersection of the tangent on the low energetic edge of the absorption spectrum with the baseline.

−5.22 and −5.23 eV, respectively. The calculated HOMO value and the band gap energy determined via UV–vis absorption were used to determine the lowest unoccupied molecular orbital (LUMO) values before and after thermal treatment, which are 3.74 and −4.01 eV, respectively. The HOMOs, LUMOs, and electron densities of P(TBPyTBIID) calculated using DFT are shown in Fig. S8, and the integrated data regarding the measured and calculated electrochemical properties are shown in Table 1.

Organic solvent/acid/UV resistances

The physicochemical properties of the P(TBPyTBIID) film before and after thermal treatment are shown in Fig. S11. The coated P(TBPyTBIID) film is stable in H_2O, CH_3OH, *i*-propyl alcohol (IPA), and hexane regardless of the thermal treatment. However, the P(TBPyTBIID) film that was not thermally treated dissolved in CF and chlorobenzene (CB) (Fig. S11a), and the film was physically peeled off in acetic acid due to degradation. However, the thermally treated film does not degrade or dissolve (Fig. S11b).

The UV resistance properties measured using a UVC 150 device from Omniscience are shown in Fig. 4a. UV with a wavelength of 253.7 nm (15–20 mW/cm^2) was irradiated for 30 min on a thin film on glass coated with P(TBPyTBIID) solution (2 mg/mL). The P(TBPyTBIID) films that are not thermally treated completely decompose under UV irradiation, with no signals observed. Conversely, the spectra of the thermally treated films partially maintain several of their absorption peaks. UV tolerance studies were conducted on films with varying concentrations (1, 2, 5, or 10 mg/mL) of P(TBPyTBIID), and the results are shown in Fig. 4b. The intensities of the peaks do not directly decrease even after UV irradiation if higher P(TBPyTBIID) concentrations (5 or 10 mg/mL) are used, which is consistent with the general decomposition mechanism of polymers. When polymers are irradiated with UV light, the carbons in the backbone form free radicals, which react with atmospheric oxygen to form C≡O, and finally C═O, thus breaking the backbone [31].

If the concentration of P(TBPyTBIID) is low, photodegradation occurs due to this mechanism, but if P(TBPyTBIID) is packed sufficiently densely at a concentration of >5 mg/mL, the formed radical recombines with another radical within the packing, which ultimately prevents the degradation of P(TBPyTBIID).

Microstructure ordering analysis

Fig. 5 shows the X-ray diffraction patterns for analyzing the crystal structure of P(TBPyTBIID).

The data of the out-of-plane mode, as shown in Fig. 5a, reveal amorphous characteristics before thermal treatment, but a high-angle, broad peak (010) corresponding to π···π stacking is observed at 24.90° after thermal treatment. Therefore, P(TBPyTBIID) likely exhibits a strong face-on structure after thermal treatment. The face-on orientation of P(TBPyTBIID) is shown in Fig. 5b. The intermolecular π···π stacking distance calculated using Bragg's Law ($\lambda = 2d \sin\theta$) is 3.57 Å. The face-on orientations of polymers efficiently transfer charges in the vertical direction [32–34]. In the case of P(TBPyTBIID), the polymer acquires a face-on structure via the cleavage of the *t*-BOC side chains during thermal treatment, and thus, when the polymer is applied to OSCs, we should observe superior photovoltaic properties compared to those of the polymer prior to thermal treatment.

Photovoltaic properties

Fig. 6a, b and Table 2 show the device structure and results of using P(TBPyTBIID) as a donor in the active layer and as a UV protection material. As shown in Table 2, the acceptor is the active

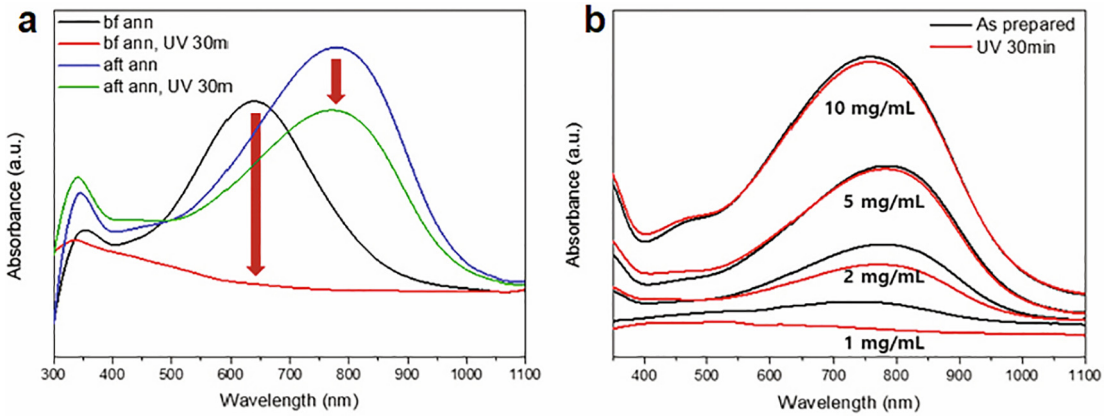

Fig. 4. a UV tolerance test of P(TBPyTBIID) films (2.0 mg/mL solution) before and after thermal annealing, b tolerance to ultraviolet ray of P(TBPyTBIID) films after thermal annealing coated with various concentrations.

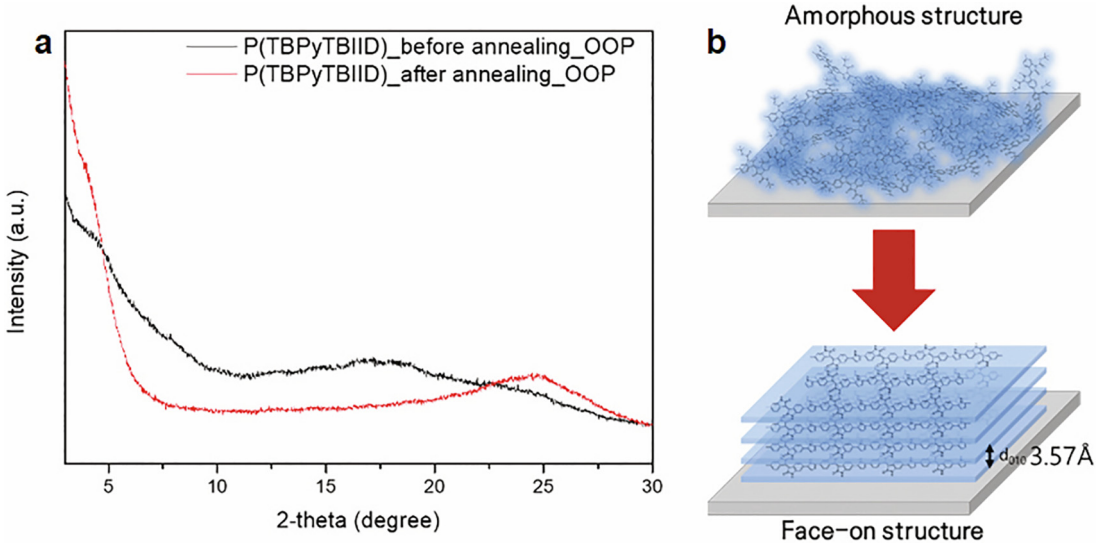

Fig. 5. (a) XRD of P(TBPyTBIID) before and after annealing in out-of-plane, and (b) schematic image of P(TBPyTBIID)'s crystallinity change after thermal annealing.

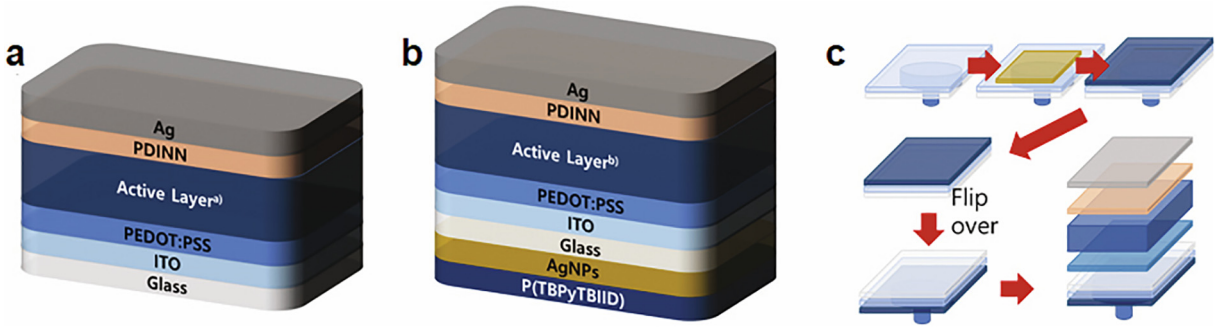

Fig. 6. (a, b) Structure of fabricated OSC devices with active layer of P(TBPyTBIID):Y6-BO-4Cl or PM6:P(TBPyTBIID):Y6-BO-4Cl[a)] and PM6:Y6-BO-4Cl[b)], (c) schematic illustration of the device fabrication procedure with extra UV-blocking layer beneath the glass substrate.

Table 2
Detailed photovoltaic performances of fabricated OSC devices under illumination of AM1.5G, 100 mW/cm^2 light.

#	Donor materials	UV-blocking layer	J_{SC} [mA/cm^2]	V_{OC} [V]	FF [%]	PCE(0) [%]	PCE(3 h)[f)]/PCE(0) [normalized]
1	P(TBPyTBIID)[a)]	None	0.64	0.68	21.9	0.10	-
2	P(TBPyTBIID)[b)]	None	1.46	0.50	41.7	0.31	-
3	PM6[a)]	None	23.54	0.79	70.5	13.08	0.46
4	PM6[a)]	AgNPs[c)]	23.63	0.79	70.6	13.23	0.49
5	PM6[a)]	AgNPs[c)] + P(TBPyTBIID)[d)]	19.98	0.76	70.4	10.64	0.51
6	PM6[a)]	AgNPs[c)] + P(TBPyTBIID)[e)]	16.76	0.73	72.2	8.81	0.52

All the active blends are made with Y6-BO-4Cl, and annealed at 100 °C, 10 min[a)] and 150 °C, 30 min[b)].
[c)]AgNPs solution was diluted 10,000 times in isopropyl alcohol.
P(TBPyTBIID) solutions were 5 mg/mL[d)], 10 mg/mL[e)] in chloroform, respectively, and annealed 30 min at 150 °C.
[f)]Photovoltaic properties of the OSC devices with UV-blocking layer weremeasured periodically under continuous illumination of AM1.5G, 100 mW/cm^2 light condition.

material, Y6-BO-4Cl, and the donor is a bulk heterojunction (BHJ) structure that uses P(TBPyTBIID) and PM6. The active layers were thermally treated for 10 min at 100 °C (#1, #3–#6) or 30 min at 150 °C (#2). These are the general thermal treatment conditions where side chains of Y6 derivatives and P(TBPyTBIID) are 100% cleaved. The active layer that was thermally treated for 10 min at 100 °C (#1) using P(TBPyTBIID) exhibits a J_{SC} of 0.64 mA/cm^2, V_{OC} of 0.68 V, FF of 21.9%, and PCE of 0.096%. However, the active layer that was thermally treated for 30 min at 150 °C (#2) exhibits a J_{SC} of 1.46 mA/cm^2, V_{OC} of 0.50 V, FF of 41.7%, and PCE of 0.31% (Fig. 7a, Table 2). The increase in PCE due to thermal treatment (from 0.1% to 0.31%) occurs due to the increase in J_{SC} and FF, which likely occurs due to the cleavage of the side chains.

Thermal treatment for 30 min at 150 °C cleaves all side chains of P(TBPyTBIID), rendering the molecular structure highly planar and forming strong π···π stacking to favor the vertical motion of the charges [35–37]. This is consistent with the results of DFT and UV–vis spectroscopy.

Y6 based acceptors generally exhibit face-on orientation, and P(TBPyTBIID) acquires a face-on orientation after side-chain cleavage, thus the orientations of the donor and acceptor harmonize and subsequently leading to an increase in PCE. In addition, the

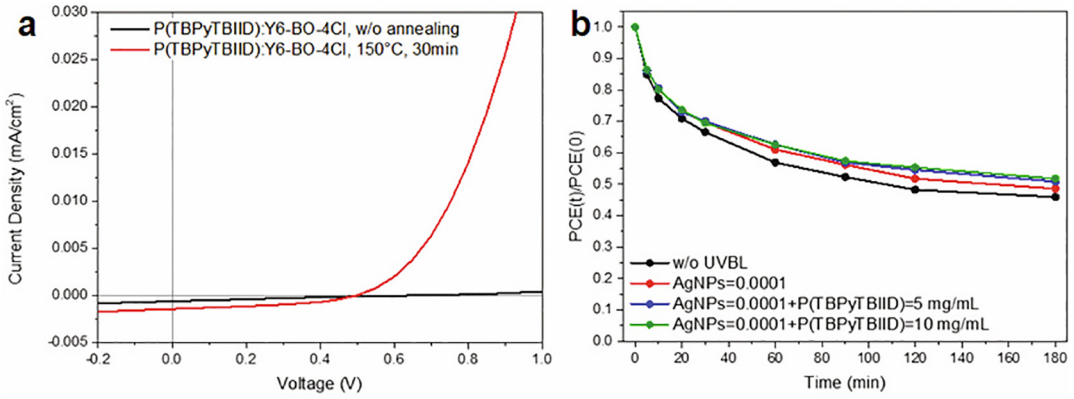

Fig. 7. (a) J-V curve of P(TBPyTBIID):Y6-BO-4Cl based device before and after thermal annealing, (b) photostability of PM6:Y6-BO-4Cl based devices with and without AgNPs and P(TBPyTBIID) as UV-blocking layer.

interchain hydrogen bonds formed during side chain cleavage promote the hopping of charge carriers.

We then manufactured and characterized a ternary device by incorporating P(TBPyTBIID) as the third component into the PM6:Y6-BO-4Cl system. We conducted thermal treatments for 10 min at 100 °C and 30 min at 150 °C to analyze the effect of side chain cleavage. Even minimal incorporation of P(TBPyTBIID) causes decreases in the V_{OC} and FF values, leading to an overall decrease in efficiency compared to that of the reference device, PM6:Y6-BO-4Cl (Table S3). This is because the incorporation of P(TBPyTBIID) damages the morphology of the BHJ formed by the PM6 and Y6-BO-4Cl blend. The incorporated P(TBPyTBIID) acts as an impurity, thus adversely affecting the morphology formed by PM6:Y6-BO-4Cl, which is confirmed by the reduction in FF. Furthermore, V_{OC} decreases upon thermal treatment at 150 °C, which also causes PCE reduction. This is also consistent with previous studies [38,39]. Stability of these PM6:P(TBPyTBIID):Y6-BO-4Cl based ternary OSCs were tested but didn't seem any improvement (Fig. S12). We then fabricated P(F-Cl):IT-4F and P(F-BiT)-COOBOCl (out):IT-4F based ternary devices[40,41] to see the generality of P(TBPyTBIID) as a third component (Fig. S14a, b, Table S8, S9). Though the device fabricating condition is not optimized, adding P(TBPyTBIID) lowered the J_{SC} dramatically, we did not further try to optimize the ternary device. According to EQE data of both ternary devices (Fig. S14 c, d), introducing P(TBPyTBIID) caused decrease of EQE throughout the whole region. The degree of EQE decrease was larger in the acceptor region than donor region, indicating that after the chain cleavage, the electrons generated at the donor cannot be transferred to acceptor efficiently.

Subsequently, we introduced P(TBPyTBIID) into the PM6:Y6-BO-4Cl system as a UV protection layer to analyze the effect on the photovoltaic characteristics. P(TBPyTBIID) may act as a UV protection layer as it blocks a certain amount of strong energy emitted by UV light. However, J_{SC} should decrease because P(TBPyTBIID) also absorbs light in the 500–1000 nm range when coated under the glass substrate. Therefore, we coated AgNPs on the bottom surface of the indium tin oxide (ITO) glass before the device was fabricated to partially compensate for the light amplification due to the surface plasmonic effect [42–47], and the subsequent increase in J_{SC} is confirmed in Table 2. AgNPs were diluted in IPA to three concentrations prior to use: 1/100, 1/1000, and 1/10000 by volume. To simultaneously act as an external protective layer for the AgNPs and a UV protection layer, P(TBPyTBIID) was further coated in concentrations of 5 or 10 mg/mL over the AgNPs, followed by thermal treatment to remove the *t*-BOC side chains. The concentration was set based on the concentration of P(TBPyTBIID) that does not decompose under UV light. P(TBPyTBIID) after side chain removal acquires strong physicochemical properties due to elevated planarity, strong π···π stacking, and interchain hydrogen bonding, therefore, the polymer acts as an external protective layer that prevents the cleavage of AgNPs, in addition to blocking UV light. The subsequent processes were conducted according to the manufacture of general OSCs by flipping the cell (Fig. 6c and S13).

For devices with incorporated AgNPs and P(TBPyTBIID) as UV protection layers, the efficiencies decrease from 10.64% to 8.81% as the concentration of P(TBPyTBIID) increases (Table 2), and the efficiencies are 19% and 33% lower compared to that of the reference device of 13.08%. The reduction in efficiency is because of the decrease in the amount of light flowing into the device due to the coating of the external surface with P(TBPyTBIID), and this is confirmed by the reduction in J_{SC}. The J_{SC} slightly increases for devices that only incorporate the AgNP layer, and the efficiency also subsequently increases slightly.

The UV protection layer was used to prevent UV-induced device degradation, and therefore, a photostability study was conducted under air for 3 h under a light source of AM 1.5G and 100 mW/cm^2 (Fig. 7b). For the reference devices, only 46% of the initial efficiencies are maintained after 3 h, but 51% and 52% of the initial efficiencies are maintained for devices coated with 5 and 10 mg/mL of P(TBPyTBIID), respectively. This improvement in stability is due to the P(TBPyTBIID) effectively blocking UV light, along with the AgNPs. The initial photovoltaic performance and photostability data of each condition are shown in Tables S4–S7. The reduction in efficiency during the first ~60 min occurs due to light-induced burn-in degradation, with the photoactive layer structurally decomposed by UV light. Several potential explanations for this burn-in degradation are proposed, but recent studies report that morphological changes caused by the UV-induced decomposition of the photoactive layer are the main causes [3,48,49]. The gradients of the graphs are not significantly different after 60 min (after burn-in degradation), but the incorporation of the UV protection layer results in enhanced stability upon comparison of the changes in the gradient before 60 min.

Conclusion

In summary, *t*-BOC side chains were linked to molecules bearing N–H groups, such as isoindigo and pyrrole, and the D–A-type polymer, P(TBPyTBIID), was synthesized via Stille coupling. The *t*-BOC chains were cleaved via thermal treatment, exposing N–H to form hydrogen bonds with the C=O of isoindigo, and enhancing the structural planarity of the polymer. Due to interchain hydrogen bonding and strong π···π stacking, the polymer exhibited strong

thermal stability and solvent resistance, in addition to resistances to acid and UV light. These characteristics of P(TBPyTBIID) could be used to effectively block UV light, along with AgNPs, when incorporated as a UV protection layer in OSCs, and this increases the photostability without significantly decreasing the efficiency. Furthermore, P(TBPyTBIID) could simultaneously act as an external protective layer, utilizing its improved mechanical strength acquired via side-chain cleavage to prevent AgNP elimination. As the degree of reduction in efficiency and improvement in stability required a trade-off, optimization of the conditions where the two factors were balanced was necessary to maximize the potential of the UV protection layer. In addition, P(TBPyTBIID) absorbed light in the 500–1000 nm range and reduced the efficiency, and thus, structural modifications to include high or low bandgaps to minimize absorption in the visible region may lead to improved results. This study is significant as we increase the potential for the commercialization of OSCs by proposing novel methods to enhance OSC stability. Furthermore, P(TBPyTBIID) acquiring self-immobilizing properties due to the removal of the *t*-BOC side chains should be useful in diverse device structures.

Declaration of Competing Interest

The authors declare that they have no known competing financial interests or personal relationships that could have appeared to influence the work reported in this paper.

Acknowledgements

This paper was supported by Konkuk University Researcher Fund in 2020, the Korea Institute of Energy Technology Evaluation and Planning (KETEP) and the Ministry of Trade, Industry & Energy (MOTIE) of the Republic of Korea (Nos. 2018201010636A, 20194010201790) and National Research Foundation of Korea (NRF) (No. 2020R1A2C2010916).

Appendix A. Supplementary data

Supplementary data to this article can be found online at https://doi.org/10.1016/j.jiec.2022.05.001.

References

[1] H. Kang, G. Kim, J. Kim, S. Kwon, H. Kim, K. Lee, Adv. Mater. 28 (2016) 7821.
[2] P. Cheng, X. Zhan, Chem. Soc. Rev. 45 (2016) 2544.
[3] L. Duan, A. Uddin, Adv. Sci. 7 (2020) 1903259.
[4] L. Wang, Y. Zhang, N. Yin, Y. Lin, W. Gao, Q. Luo, et al., Sol. Energy Mater. Sol. Cells 157 (2016) 831.
[5] X. Song, G. Liu, P. Sun, Y. Liu, W. Zhu, J. Phys. Chem. Lett. 12 (2021) 10616.
[6] Q. An, F. Zhang, W. Gao, Q. Sun, M. Zhang, C. Yang, et al., Nano Energy 45 (2018) 177.
[7] J. Yin, W. Zhou, L. Zhang, Y. Xie, Z. Yu, J. Shao, et al., Macromol. Rapid Commun. 38 (2017) 1.
[8] X. Song, K. Zhang, R. Guo, K. Sun, Z. Zhou, S. Huang, et al., Adv. Mater. 2200907 (2022) 2200907.
[9] X. Song, P. Sun, D. Sun, Y. Xu, Y. Liu, W. Zhu, Nano Energy 91 (2022) 106678.
[10] A. Uddin, M.B. Upama, H. Yi, L. Duan, Coatings 9 (2019) 1.
[11] H. Sun, J. Weickert, H.C. Hesse, L. Schmidt-Mende, Sol. Energy Mater. Sol. Cells 95 (2011) 3450.
[12] J.B. Patel, P. Tiwana, N. Seidler, G.E. Morse, O.R. Lozman, M.B. Johnston, et al., Mater. Interfaces 11 (2019) 21543.
[13] I.V. Martynov, A.V. Akkuratov, S.Y. Luchkin, S.A. Tsarev, S.D. Babenko, V.G. Petrov, et al., Mater. Interfaces 11 (2019) 21741.
[14] J. Jeong, J. Seo, S. Nam, H. Han, H. Kim, T.D. Anthopoulos, et al., Adv. Sci. 3 (2016) 1.
[15] Y.W. Han, S.J. Jeon, H.S. Lee, H. Park, K.S. Kim, H.W. Lee, et al., Adv. Energy Mater. 9 (2019) 1.
[16] J. Freudenberg, D. Jänsch, F. Hinkel, U.H.F. Bunz, Chem. Rev. 118 (2018) 5598.
[17] H. Zhang, K. Yang, C. Chen, Y. Wang, Z. Zhang, L. Tang, et al., Polymer (Guildf) 149 (2018) 266.
[18] Z.H. Guo, N. Ai, C.R. McBroom, T. Yuan, Y.H. Lin, M. Roders, et al., Polym. Chem. 7 (2016) 648.
[19] M. Gsänger, J.H. Oh, M. Könemann, H.W. Höffken, A.M. Krause, Z. Bao, et al., Angew. Chem. - Int. Ed. 49 (2010) 740.
[20] R. Stalder, J. Mei, K.R. Graham, L.A. Estrada, J.R. Reynolds, Chem. Mater. 26 (2014) 664.
[21] Y. Zou, X. Ji, J. Cai, T. Yuan, D.J. Stanton, Y.H. Lin, et al., Chem 2 (2017) 139.
[22] C. Liu, S. Dong, P. Cai, P. Liu, S. Liu, J. Chen, et al., Mater. Interfaces 7 (2015) 9038.
[23] K. Nakabayashi, H. Otani, H. Mori, Polym. J. 47 (2015) 617.
[24] C.K. Trinh, H.J. Lee, J.W. Choi, M. Shaker, W. Kim, J.S. Lee, New J. Chem. 42 (2018) 2557.
[25] M. Shaker, B. Park, J.H. Lee, W. Kim, C.K. Trinh, H.J. Lee, et al., RSC Adv. 7 (2017) 16302.
[26] A.O. Weldeab, A. Steen, D.J. Starkenburg, J.S.D. Williams, K.A. Abboud, J. Xue, et al., J. Mater. Chem. C 6 (2018) 11992.
[27] R. Li, C. Li, M. Liu, P. Vivo, M. Zheng, Z. Dai, et al., CCS Chem. (2021) 3309.
[28] M.A. Uddin, T.H. Lee, S. Xu, S.Y. Park, T. Kim, S. Song, et al., Chem. Mater. 27 (2015) 5997.
[29] S. Wood, J.H. Kim, J. Wade, J.B. Park, D.H. Hwang, J.S. Kim, J. Mater. Chem. C 4 (2016) 7966.
[30] S. Sasaki, G.P.C. Drummen, G.I. Konishi, J. Mater. Chem. C 4 (2016) 2731.
[31] T. Lu, E. Solis-Ramos, Y. Yi, M. Kumosa, Polym. Degrad. Stab. 154 (2018) 203.
[32] S. Li, B. Zhao, Z. He, S. Chen, J. Yu, A. Zhong, et al., J. Mater. Chem. A 1 (2013) 4508.
[33] H. Mori, Polym. J. 53 (2021) 975.
[34] H. Mori, Y. Nishihara, Polym. J. 50 (2018) 615.
[35] M.H. Choi, E.J. Ko, Y.W. Han, E.J. Lee, D.K. Moon, Polymer (Guildf) 74 (2015) 205.
[36] T.H. Lee, M.H. Choi, S.J. Jeon, D.K. Moon, Polymer (Guildf) 99 (2016) 756.
[37] S.J. Jeon, Y.W. Han, D.K. Moon, ACS Appl. Mater. Interfaces 11 (2019) 9239.
[38] J. Yuan, Y. Zhang, L. Zhou, G. Zhang, H.L. Yip, T.K. Lau, et al., Joule 3 (2019) 1140.
[39] Y. Cui, H. Yao, J. Zhang, T. Zhang, Y. Wang, L. Hong, et al., Nat. Commun. 10 (2019) 1.
[40] S.J. Jeon, Y.W. Han, Y.H. Kim, D.K. Moon, Sol. RRL 4 (2020) 1.
[41] S.J. Jeon, Y.H. Kim, D.H. Hong, N.G. Yang, Y.W. Han, D.K. Moon, Sol. RRL 5 (2021) 1.
[42] A. Uddin, X. Yang, J. Nanosci. Nanotechnol. 14 (2014) 1099.
[43] T. Putnin, C. Lertvachirapaiboon, R. Ishikawa, K. Shinbo, K. Kato, S. Ekgasit, et al., Opto-Electronic Adv. 2 (2019) 190010.
[44] C.R. Singh, T. Honold, T.P. Gujar, M. Retsch, A. Fery, M. Karg, et al., Phys. Chem. Chem. Phys. 18 (2016) 23155.
[45] K. Chan, M. Wright, N. Elumalai, A. Uddin, S. Pillai, Adv. Opt. Mater. 5 (2017) 1600698.
[46] S. Phetsang, S. Nootchanat, C. Lertvachirapaiboon, R. Ishikawa, K. Shinbo, K. Kato, et al., Nanoscale Adv. 2 (2020) 2950.
[47] L. Feng, M. Niu, Z. Wen, X. Hao, Polymers (Basel) 10 (2018) 1.
[48] E. çetin Yilmaz, M.K. Yeşilyurt, I.V. Öner, G. Ömeroğlu, A.N. Özakin, Period. Eng. Nat. Sci. 5 (2017) 152.
[49] Q. Burlingame, X. Huang, X. Liu, C. Jeong, C. Coburn, S.R. Forrest, Nature 573 (2019) 394.